

# Two-dimensional wave patterns of spreading depolarization: retracting, re-entrant, and stationary waves <sup>☆</sup>

Markus A. Dahlem<sup>\*,a,b,c</sup>, Rudolf Graf<sup>d</sup>, Anthony J. Strong<sup>e</sup>, Jens P. Dreier<sup>f</sup>, Yuliya A. Dahlem<sup>f,g</sup>, Michaela Sieber<sup>g</sup>, Wolfgang Hanke<sup>g</sup>, Klaus Podoll<sup>h</sup>, Eckehard Schöll<sup>a</sup>

<sup>a</sup>Institut für Theoretische Physik, Technische Universität Berlin, Berlin, Germany

<sup>b</sup>Department of Neurology, Otto-von-Guericke-University Magdeburg, Magdeburg, Germany

<sup>c</sup>Leibniz Institute für Neurobiologie, 39118 Magdeburg, Germany

<sup>d</sup>Max Planck Institute for Neurological Research, Cologne, Germany

<sup>e</sup>Kings College London, Department of Clinical Neuroscience, Institute of Psychiatry, United

<sup>f</sup>Department of Neurology, Charité Campus Mitte, Berlin, Germany

<sup>g</sup>University of Hohenheim, Membrane Physiology, Stuttgart, Germany

<sup>h</sup>Department of Psychiatry and Psychotherapy, RWTH Aachen University, Aachen, Germany

## Abstract

We present spatio-temporal characteristics of spreading depolarizations (SD) in two experimental systems: retracting SD wave segments observed with intrinsic optical signals in chicken retina, and spontaneously occurring re-entrant SD waves that repeatedly spread across gyrencephalic feline cortex observed by laser speckle flowmetry. A mathematical framework of reaction-diffusion systems with augmented transmission capabilities is developed to explain the emergence and transitions between these patterns. Our prediction is that the observed patterns are reaction-diffusion patterns controlled and modulated by weak nonlocal coupling. The described spatio-temporal characteristics of SD are of important clinical relevance under conditions of migraine and stroke. In stroke, the emergence of re-entrant SD waves is believed to worsen outcome. In migraine, retracting SD wave segments cause neurological symptoms and transitions to stationary SD wave patterns may cause persistent symptoms without evidence from noninvasive imaging of infarction.

**Key words:** pattern formation, reaction-diffusion, spiral waves, migraine, stroke

## 1. Introduction

The World Health Organization lists migraines among the four most disabling chronic medical disorders [1]. Stroke is currently the third leading cause of death in developed countries. There is clinical and experimental evidence that in both conditions spreading depolarization (SD) waves of non-or-all type emerge. SD waves are characterized by massive redistribution of ions across cell membranes peaking after several seconds in a nearly complete neuronal depolarization, followed by a much slower recovery process taking up to minutes during which ion gradients are re-established towards their physiological values. This maximal ionic perturbation clearly distinguishes SD from all other brain states such as epileptic seizure activity, functional activation or the physiological resting state. The sequence of ionic perturbation and its recovery spreads at a pace of about 3 mm/min over cortical regions.

In migraine, this phenomenon—originally termed *spreading depression* of activity in the cerebral cortex [2], causes neurological symptoms starting about 30 min before the headache phase [3, 4, 5]. It is also currently debated whether migraine headache is caused by substances released in the course of SD

[6]. In stroke, so-called *periinfarct depolarizations* [7], a variant of SD, occur and spread in the boundary zones surrounding a cerebral infarct. A greater number of SD waves is believed to worsen outcome. SD has been demonstrated in patients suffering from traumatic brain injury, ischemic stroke, subarachnoid haemorrhage and intracerebral haematoma [7, 8, 9, 10, 11].

The difference between SD in migraine and stroke is that SD in the latter occurs when the cortex is deprived of adequate perfusion, i. e., under ischemia, while SD in migraine occurs under normoxic conditions, but otherwise both processes share a common underlying neuronal mechanism [12], and they should not be seen as two different processes. For this reason they are referred to as *spreading depolarizations* [10]. This name reflects the common mechanism rather than the effect (depression of activity) or location (periphery of infarct) of these waves as the other terms do. To focus on common macroscopic features is in particular advisable when two-dimensional spatio-temporal characteristics are investigated. Moreover, it emphasises the depolarization wave as one of the common aspects within the complex bidirectional relation between migraine and stroke [13, 14]. For example, SD activity may play an important role in complications of migraine, including migrainous infarction, persisting migraine aura without infarction, and ischaemia-induced migraine (symptomatic migraine).

In this study, our aim is to understand the emergence of

<sup>☆</sup>Special issue: Emerging Phenomena.

\*Corresponding author, dahlem@physik.tu-berlin.de

pathological spatio-temporal SD states in the cortex and possible transitions between them in terms of nonlinear dynamics and pattern formation. This approach complements more traditional clinical research methodologies. The paper is organized as follows. In Sec. 2, we introduce the experimental setup, followed by a description of the observed patterns in Sec. 3. In Sec. 4, we propose a mathematical framework to model reaction-diffusion patterns that are controlled and modulated by weak nonlocal transmission, and in Sec. 5 we illustrate the applicability of this concept by special cases derived from this framework. We end with a discussion in Sec. 6.

## 2. Methods and Materials

Monitoring the spatio-temporal characteristics of SD in two spatial dimensions is crucial for studying this phenomenon, in particular from a clinical point of view. We present data from two experimental systems of complementary complexity each with a specific optical method. Optical methods have much better spatial resolution than electrical measurements. They provide indirect evidence of SD. The information about the spatio-temporal development of SD is very precise since correlation between the optical signals and electrophysiological changes of SD are well studied [15, 16, 17].

### 2.1. Chicken retina as SD model

The chicken retina is a typical *in vitro* system used to study the formation of pathological activity pattern of SD by intrinsic optical signals [18, 19]. Retinal SD can be easily observed by intrinsic optical signals, because it evokes an optical signal with an amplitude being several orders of magnitude higher than that observed in cortex. In fact, retinal SD can be observed by the naked eye as a milky front. Moreover, the chicken retina is a very homogeneous neural tissue because it lacks blood vessels. The neural aspects of pattern formation can be thus studied in retinal SD in isolation, that is, without the neurovascular coupling, with the obvious disadvantage that retinal SD provides no information on this coupling. Last but not least, the retina has, similar to the cortex, a layered structure with several layers of neurons interconnected by synapses and there is a solid knowledge of retinal network functioning [20].

The chickens (4-7 days) were decapitated and the eyes were carefully extracted from the orbit. The eye was purged from adherent muscles and connective tissue and afterwards the eye was equatorially divided. The vitreous body was gently removed, and then the eyecup including the retina was transferred into a small petri-dish filled with standard Ringer (R) solution (Fig 1 (a)). The standard Ringer solution has the following composition (in *mM*): 100 *NaCl*, 6 *KCl*, 1 *CaCl<sub>2</sub>*, 1 *MgSO<sub>4</sub>*, 30 *NaHCO<sub>3</sub>*, 1 *NaH<sub>2</sub>PO<sub>4</sub>*, 30 glucose. Throughout the experiment, the submerged retina was perfused with fresh Ringer solution. For more details see Ref. [18].

Following this preparation protocol, the healthy chicken retina has a dark appearance. Since blood vessels do not course across the retinal surface, the only landmark, situated in the infero-temporal field, is the pecten oculi (Fig 1 (b)), a highly vascularized organ with corrugated structure that projects from the optic

disc into the vitreous body of the avian eye. The pecten is believed to nourish the retina. Pectineal blood capillaries deliver nutrients to the retina, therefore, there are no retinal blood vessels. This fact, together with the intrinsic optical signal, makes the avian retina an ideal experimental system to study SD.

All measurements were obtained with a CCD video camera and stored with a DVD-recorder. The retina was pricked with a fine Tungsten needle to elicit a retinal SD wave. After measuring a control wave, the standard Ringer solution was replaced with a Ringer solution where drugs had been added. After a time of 30 minutes a new wave was elicited. The experiments in chicken retina were approved by the local ethics committee (Stuttgart and Magdeburg) and the Regierungspräsident of Stuttgart and Magdeburg.

### 2.2. Stroke model

The choice of the cat as a species for studying SD has been governed by disappointing experience with the use of rodent models of stroke: none of the promising trials of neuroprotective agents in rodents, especially those that block SD, has been reproduced in clinical trials of the same agent. The cat cortex is closer than rodent cortex to that of humans in two important respects. First, it is gyrencephalic (folded), whereas the rodent cortex is lissencephalic (smooth). The data obtained establish beyond doubt that SD spreads via sulci (clefts between gyral convexities), and never "jumps" between gyral convexities; the information has allowed reliable interpretation of data from monitoring the human brain, and indeed provided a justification for the initial work (with invasive monitoring methods) seeking evidence of depolarisations in the injured human brain. Secondly, the ratio of astrocytes to neurones in the cat brain is much closer to that of the human brain than it is in the rodent brain. This is important since the small energy metabolite pool in the brain, glycogen, is almost entirely located in astrocytes, again making a model of occlusive stroke in cats a more reliable analogue of human stroke than one in rodents. A further advantage of the cat brain is that the anatomical arrangement of its blood supply closely resembles that of the human brain.

In cat cortex, SD can be visualized by illuminating the cortex with laser light and imaging the resulting speckle pattern. The laser speckle contrast imaging can be used as a proxy for SD, because cerebral blood flow changes are almost invariably coupled to SD and so these changes can be studied as surrogate markers to image and map the occurrence and spread of SD in real time [16]. The imaging observation field was chosen so as to achieve maximal spatial resolution in the area around the periphery of the initial stimulation site. Fig. 3 (a) illustrates the anatomy of the cat cerebral cortex, where the gyri are arranged in concentric arcs, in the order ectosylvian (EG), suprasylvian (SG), marginal (MG) gyri. The experiments in cats were approved by the local ethics committee and the Regierungspräsident of Cologne.

## 3. Experimental results

In the following two subsections, we present the observed SD patterns in two experimental systems. We then develop in

Sec. 4 the conceptual framework for modeling SD on a macroscopic level that allows us to understand these experimentally observed spatio-temporal patterns of SD and possible transitions between them in terms of nonlinear dynamics. In Sec. 5, special cases are derived from this framework.

### 3.1. Retracting retinal SD waves segments

An SD wave segment is a wave with a broken wave front and thus with two freely moving open ends. The open ends of the wave front allow more complex spatio-temporal dynamics, in contrast to a wave with a closed wave front or a wave where the open ends are attached to a non-excitable boundary. Monitoring the dynamics of the open ends can be used to probe the tissue excitability, as we will first show experimentally and then develop the mathematical framework in the next section.

Travelling SD wave segments have, to our knowledge, neither been observed in cortex nor in any other grey matter brain region of any species. However, indirect evidence, presented in a recent study combining migraine patients' reports and high-field functional magnetic resonance imaging, suggests that retracting SD wave segments cause migraine aura symptoms [21]. We show here that these retracting waves can be observed in retinal SD by controlling excitability in a regime weakly susceptible to SD. This provides the first direct evidence that the recently predicted retracting waves exist in SD and that their emergence depends critically on the tissue excitability.

An SD wave segment can be created from an initially closed circular SD wave front. The circular SD wave is created by local superthreshold stimulation. One way to break the SD front is by manually inducing a transient excitation block in the tissue in some confined location in front of the approaching wave. Performing this procedure, the two open ends of the wave segment usually curl in to form a double spiral, whose wave front then repeatedly re-enters the same retinal tissue. In chicken retina, a spiral-shaped SD can rotate up to 20 times before its center collides with the tissue boundary [22]. Another way to obtain wave segments is to reduce retinal susceptibility to SD to a degree at which the wave front spontaneously breaks. In this case, the newly emerged open ends retract, as we show, and the wave vanishes invading the tissue only once.

Firstly, we describe the manual creation of a spiral-shaped SD wave to contrast this procedure and the resulting spatio-temporal development with retracting SD wave segments. Retinal SD is elicited mechanically by gently touching the tissue with a sharp needle. In Fig. 1 (c), the stimulation needle (S) is seen by its dark shadow. After about 15 s, when the extension of the circular SD wave front has grown in diameter to about 0.75 mm, we administer locally through a pipette a 0.5 ml drop of Ringer solution containing a tenfold raised  $Mg^{2+}$  concentration ( $[Mg^{2+}]_R = 10 mM$ ). Pipettes having an inner tip diameter of about 0.5 mm are best suited. They must be placed directly over the surface of the submerged retina without touching it and less than 1 mm in front of the approaching SD wave (Fig. 1 (e)). For visual guidance, the contours of the pipettes, which is out of focus in Fig. 1 (e), is indicated by dashed lines and its target position marked by an asterisk. The propagation of the circular SD wave is blocked around the pipette's target position and as

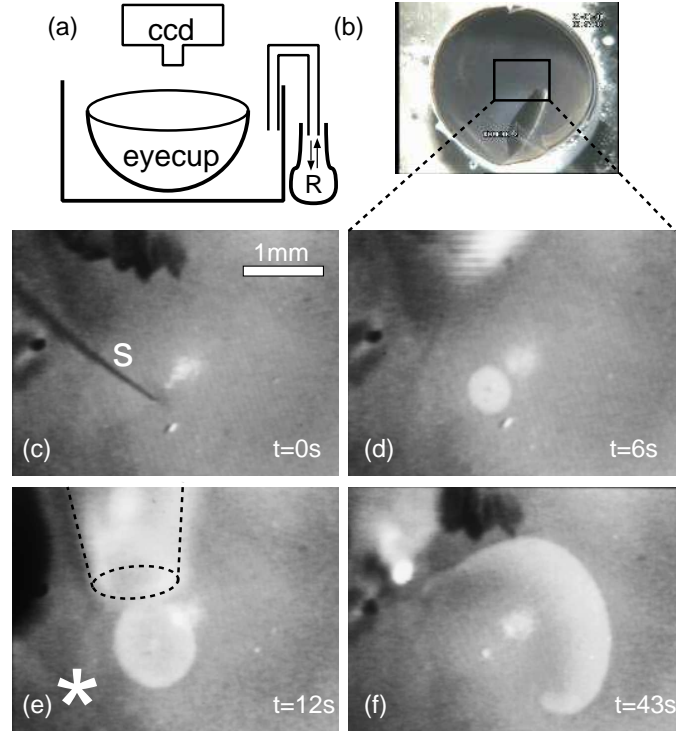


Figure 1: Creation of a retinal SD wave segment with freely revolving open ends: (a) scheme of experimental set up with eyecup preparation placed in a petri-dish, perfused with Ringer (R) solution and monitored by a CCD camera; (b) top view image from eyecup; (c) mechanical stimulation with sharp needle S; (d) circular SD wave, (e) local administration of  $Mg^{2+}$  via pipette indicated by dashed lines at location marked by an asterisk; (f) retinal SD wave segment.

a consequence its wave front breaks open. This wave segment develops into a spiral-shaped wave (Fig. 1 (f)), if the submerged retina is kept in standard Ringer solution and one end attaches to the tissue boundary of the retina.

We now adjusted retinal susceptibility to SD by adding cocaine in a 1 – 3 mM concentration range in 1 mM concentration steps. At 1 mM cocaine concentration, SD waves propagated normally after being stimulated mechanically. At 2 mM cocaine concentration, we observed a spontaneous excitation block. In Fig. 2 (c), this happens at a location where the retina appearance was less dark indicating a compromised tissue state. The tissue at this location is, however, still viable. After the cocaine is washed out, SD waves propagate normally again in the entire retina. The open ends of the SD wave segment retracts in the further course (Fig. 2 (d)-(f)). In Fig. 2 (b)-(f), we manually and individually enhanced the brightness and contrast in rectangular regions of interest to better visualize the SD wave. Furthermore, in figures (Fig. 2 (g)-(l)) the spatio-temporal development is schematically shown in a drawing.

The retinal susceptibility to SD was at 2mM cocaine concentration already so low, that in most cases the initiated wave collapsed after spreading only a short distance. The term *collapse* refers to an unstable, and therefore transient, SD wave profile that fades away although the front does not break. This

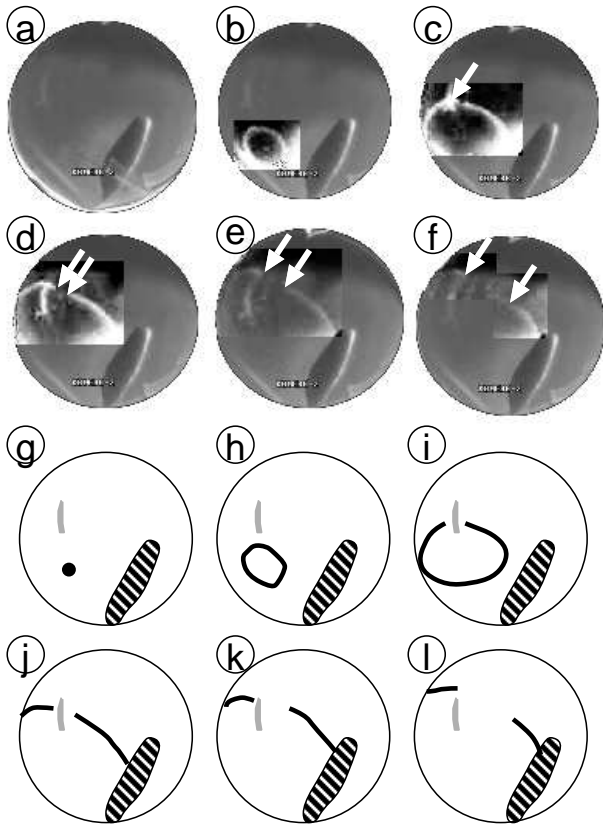


Figure 2: Six snapshots taken at 40 s time interval from chicken retina. (a)-(f) original recordings from CCD camera with enhanced brightness and contrast in rectangular regions of interest. White arrow in (c) marks the breaking of the retinal SD wave, and subsequent pair of white arrows in (d)-(f) mark the location of the open ends of retinal SD wave. (g)-(l) Schematic illustration of this sequence. Retinal SD wave shown as black line, tissue in a compromised but viable state is marked gray, and pecten is shown filled with stripe pattern.

process was predicted for SD to occur extremely close to the susceptibility range of retracting waves segments [23]. At  $3mM$  cocaine concentration retinal SD waves could not be elicited anymore. Retracting retinal SD waves have also been observed by reducing the potassium concentration in Ringer from  $[K^+]_R = 6mM$  to values between  $1 - 2mM$ . For concentrations below  $[K^+]_R = 3mM$ , the intrinsic signal of the retinal SD wave profile changes in a characteristic way [24], and the condition of the retina was hardly stable for more than 30 min. Therefore no control measurement perfusing the retina with standard Ringer could be done.

### 3.2. Re-entrant cortical SD waves

A single SD wave that repeatedly invades the same tissue forms a re-entrant pattern. A re-entrant pattern is easy to understand as a wave propagating around an obstacle. This obstacle can be a functional or anatomical block. In this subsection, we present re-entrant SD patterns revolving around an anatomical block that develops after microinjections of high concentration of potassium have been locally administered to the cortical surface. Firstly, we describe further in the next paragraph functional blocks in SD and re-entrant spiral patterns, whose cre-

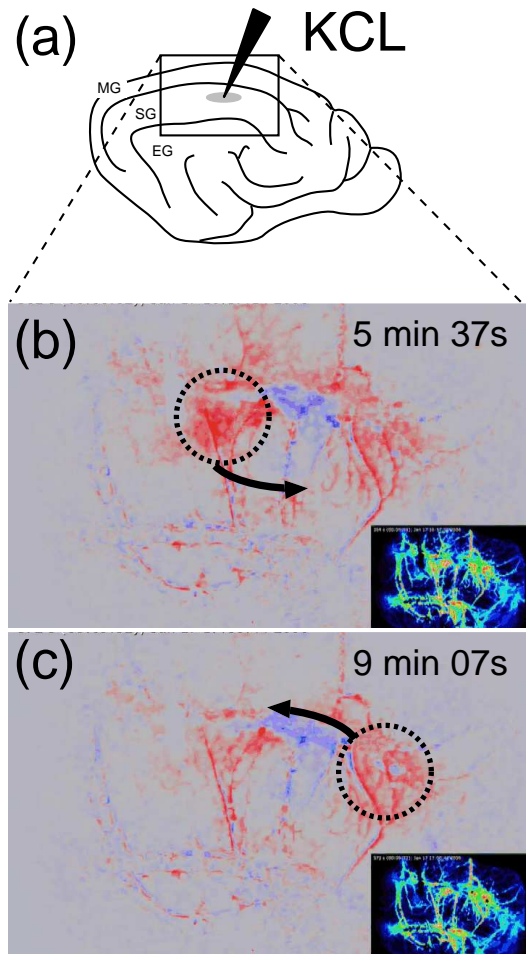


Figure 3: (a) Diagram of the lateral aspect of the right hemisphere of the cat brain illustrating typical gyral anatomy of a small ischaemic area (gray) within the area exposed for imaging (rectangle). (b) Following *KCL* injection (at  $t=0$ ), and an immediate transient radially spreading wave from the injection site, a new single wave of hyperemia appears spontaneously and cycles anticlockwise 3.5 times around an injured area of some  $3 - 5mm$  diameter centred on the original injection site, and commencing medial to it (above as viewed in this image field). Two snapshots were taken at a 3.5 min interval. The reader is advised to run the video to see the patterns.

ation protocol was introduced in the previous subsection (Fig. 1 (f)).

A functional block refers to a block that transiently forms as an intrinsic property of the 2D wave dynamics. The core of the rotating spiral center in retinal SD is an example of a functional block. Since re-entrant SD waves with a functional block in the cortex have, to the best of our knowledge, not been reported, we refer here to the observed characteristics in the retinal experiments. The spiral core can be a circular area under certain conditions, but it is in general a more complex structure. For example, the core does not need to cover a spatially extended two-dimensional area, instead it can be an one-dimensional curved line (inset (a) Fig. 5), which itself performs a rotation, as is the case for retinal SD [22]. The detailed dynamics of the core is a measure of susceptibility to SD and provides important information about macroscopic model parameters (see Sec. 4.6).

In contrast to a functional block, an anatomical block refers

to non-excitable tissue, possibly an infarct region or an artificially created lesion. SD patterns rotating around an artificially created lesion have also been called reverberation of SD waves [25]. Reverberation of SD was demonstrated in rat cerebral cortex and has been known for a long time. Recently, data from monitoring the human brain has renewed interest in re-entrant patterns [11], in particular in experimental models of stroke to investigate the cause of infarct expansion, because more frequent SD waves are believed to worsen stroke outcome and therefore the emergence of re-entrant SD waves is of considerable clinical interest.

The creation of a re-entrant wave demands, in general, special initial conditions. SD is induced with microinjections into the cortex of 1 M potassium chloride (*KCl*). As described in Sec. 2.2, laser speckle contrast imaging flowmetry is used to detect waves of regional blood flow alteration coupled to SD in a cortical field of view covering three gyri called marginal, suprasylvian, and ectosylvian gyrus (MG, SG, and EG) respectively (Fig. 3 (a)). A radial pattern is regularly observed for the initial wave after an injection, starting from the point of *KCl* injection and propagating outwards, often appearing as a concentric wave. This is demonstrated with a supplementary video (Video 1, filename dahlemEtAlVideo.mov).

Following the radial pattern, an area of markedly reduced perfusion becomes established surrounding the injection point. We infer that an ischemic region develops at this site, most likely due to the marked vasoconstriction associated with high levels of  $K^+$  concentration in the perivascular fluid. It is known that the perivascular administration of  $K^+$  concentrations at levels of 40 mM decreases pial arteries calibre by 47.2% and vein calibre by 13.5% [26]. This significant reduction changes the conditions at the injection point and in its border zone. At least this assumption is consistent with the changes following the radial pattern and being observed in the surrounding of this developing ischemic focus.

During observation for 40 minutes following a *KCl* injection, we saw new waves of hyperemia that developed spontaneously at the edge of the lesion, without any further *KCl* injection. Surprisingly, these secondary waves did not propagate radially but instead each revolves several times the ischemic focus. This is demonstrated in the supplementary video (Video 1, filename dahlemEtAlVideo.mov). Similar perilesion re-entrant patterns have been seen around experimental ischaemic lesions in the cerebral cortex after occlusion [17]. Furthermore, note that re-entrant patterns result in consistent periodicity of depolarizations when monitored at a single cortical point, and such periodic events have also been seen in the injured human brain [11].

#### 4. Augmented reaction-diffusion model

In this section, we develop the conceptual framework for modeling SD on a macroscopic level. This framework consists of a continuum model of the cortex in which the communication between neurons is separated in two major schemes: (i) local coupling, and (ii) nonlocal coupling in space and time. In the cortex, these schemes represent (i) diffusion, and (ii) network

communication and neurovascular feedback. With this framework general information is gained on how reaction-diffusion patterns of pathological states in the cortex are controlled and modulated by weak nonlocal transmission schemes. We apply this framework in Sec. 5 to interpret the experimentally observed patterns, in particular, their emergence and transitions.

##### 4.1. Model equation

The level of detail and complexity of our framework is determined by both spatial extension and propagation speed of the emerging patterns. SD waves extend in the cortex over several centimeters and spread with a remarkably slow speed of several millimeters per minute. The extension of SD patterns suggests that its mathematical description should be in terms of large-scale activity in neural populations and describe how this activity affects the cortical ionic equilibrium (homeostasis). The slow speed of SD (about  $3 \text{ mm min}^{-1} = 50 \mu\text{m s}^{-1}$ ) indicates that diffusion in cortical tissue plays a major role. Therefore, the central parts of a macroscopic continuum model of SD are reaction rate terms and diffusion terms. These terms are supplemented by additional terms reflecting augmented transmission capabilities. Within such a framework, the model equation is

$$\begin{pmatrix} \partial_t u \\ \varepsilon^{-1} \partial_t v \end{pmatrix} = \begin{pmatrix} f(u, v) \\ g(u, v) \end{pmatrix} + \mathbf{D} \begin{pmatrix} u \\ v \end{pmatrix} + \mathbf{H} \begin{pmatrix} u \\ v \end{pmatrix}, \quad (1)$$

where  $\partial_t$  is a short hand notation for the derivative with respect to time. The terms on the right hand side represent (i) reaction rates  $f(u, v)$  and  $g(u, v)$  of a simplified activator( $u$ )-inhibitor( $v$ ) model of cortical homeostasis (Sec. 4.2), (ii) diffusion of chemical signals and other local transmission schemes summarized under the term *volume transmission* in the brain and described by the diffusion operator  $\mathbf{D}$  (Sec. 4.3), and (iii) the augmented transmission capabilities described by an operator  $\mathbf{H}$  (Sec. 4.4). The model equation (1) and also its derived special cases (Sec. 5) are nondimensionalized equations. In such systems, natural units of a system are used in a systematic manner so that the input and output variables of the rate functions  $f(u, v)$  and  $g(u, v)$  are in the order of unity. Therefore, beside many other advantages, nondimensionalization suggests explicitly a parameter, namely  $\varepsilon$  that should be used for analyzing this pattern forming system. The parameter  $\varepsilon$  indicates how much slower the production rate of the inhibitor  $v$  is compared to the one of the activator  $u$ .

##### 4.2. Activator-inhibitor dynamics

Local dynamics of activator-inhibitor type are common in pattern forming systems, and—if they are coupled by diffusion—have been shown to govern several aspects of SD wave propagation [27, 28, 29, 30, 31]. The reaction rates  $f(u, v)$  and  $g(u, v)$  in Eq. (1) represent such simplified local dynamics in the cortical ion homeostases (see Fig. 4) leading to non-or-all type behavior (excitability). The rate function  $f(u, v)$  describes the change in a proxy agent named activator  $u$  by lumping together nonlinear reactions containing a positive feedback loop in the SD mechanism, such as  $Na^+$ -inward currents (dashed arrows

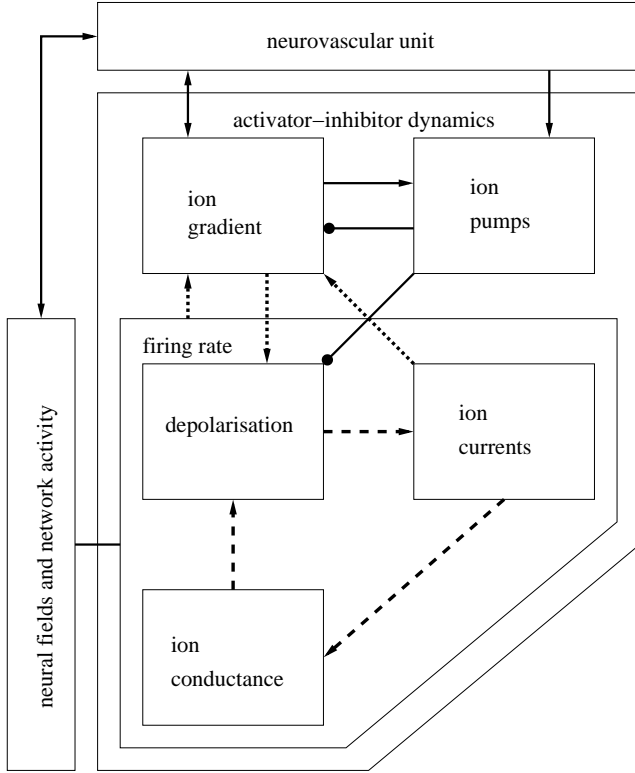


Figure 4: Flow chart of feedback loops and transmission pathways in SD.

in Fig. 4) and extracellular potassium concentration  $[K^+]_e$  (dotted arrows). Likewise, the rate function  $g(u, v)$  of the inhibitor  $v$  represents recovery processes, such as effective regulation of  $[K^+]_e$  and pump currents by the neuron's electrogenic  $Na^+-K^+$  ion pump (solid arrows with circular heads).

An activator-inhibitor system exhibiting excitability requires a certain configuration of trajectories that follow the vector field given by the functions  $f(u, v)$  and  $g(u, v)$  in the phase space [32, 33]. This configuration usually results from the parameter vicinity of an oscillatory regime whose large amplitude limit cycle is suddenly destroyed. A rest state (fixed point) is usually the only attractor in the excitable regime. There exists also a threshold close to this rest state, e. g., a separatrix or a sharp trajectory, that must be crossed by a stimulation to result in phase space excursion. Activator-inhibitor systems are the most generic systems to exhibit such behavior. A particular example is derived in Sec. 4.5 and the validity and applicability of generic dynamics to model SD is discussed in Sec. 6.

### 4.3. Volume transmission

Communication between neurons is usually classified in two schemes: wiring and volume transmission [34]. Volume transmission is mainly characterized by diffusion of chemical signals in the extracellular space. That diffusion is the main cause of the spread in SD is indicated by the propagation speed of about  $50 \mu m s^{-1}$ . Waves caused by nonlinear reactions coupled by diffusion of monovalent ions travel at speeds in the order of  $10 \mu m s^{-1}$  assuming moderate reaction rates in the nonlinear

dynamics [31]. Signals transmitted by cortical wiring, in particular action potential along axons, travel at speeds in the order of meters per second, i. e., five orders of magnitude faster.

The diffusion operator in Eq. (1) and takes the general form

$$\mathbf{D} = \begin{pmatrix} 1 & 0 \\ 0 & \lambda \end{pmatrix} \nabla^2, \quad (2)$$

with  $\nabla^2$  being the Laplace operator. We do not consider cross-diffusion, therefore off-diagonal entries vanish. The foam-like geometry of the interstitial space renders diffusion in the brain different from aqueous solution. In particular, apparent diffusion coefficients should be considered in a dimensionalized model [35]. In our nondimensionalized framework, diffusion coefficients of activator and inhibitor,  $D_u$  and  $D_v$ , respectively, do not appear explicitly. Only the ratio  $\lambda = \frac{D_v}{\varepsilon D_u}$  of the diffusion coefficients enters Eq. (2) as a parameter (note that  $\varepsilon$  appears also in this quotient). In SD, inhibitory reactions are thought to relate to ion pump activity (Fig. 4), in which case the inhibitor would not be subject to diffusion and therefore we choose  $\lambda = 0$  in this study.

### 4.4. Augmented transmission

Similar to the diffusion operator in Eq. (2), the operator  $\mathbf{H}$  describes the augmented transmission capabilities as

$$\mathbf{H} = K \begin{pmatrix} A_{uu} & A_{uv} \\ A_{vu} & A_{vv} \end{pmatrix} F. \quad (3)$$

$F$  is a operator specifying the augmented transmission (in analogy to the Laplace operator  $\nabla^2$  for volume transmission), examples are given in Sec. 5. The four elements of the matrix  $A_{ij}$  specify the relative coupling strength among different schemes of augmented transmission (in analogy to  $\lambda$  in Eq. 2) so that the operator  $A_{ij}F$  represents three individual steps of augmented transmission, namely (I) selecting a species  $j$  whose transmission capability is augmented, (II) creating the nonlocal driving force from this species, and (III) feeding this driving force back, multiplied by the coupling strength  $K$ , into the dynamical variable of species  $i$ , with  $i, j \in \{u, v\}$ .

The parameter  $K$  describes the coupling strength relative to the diffusion coefficient, which is normalized to unity. Therefore, the  $A_{ij}$  are also normalized to unity, i. e.,

$$\max(\{|A_{uu}|, |A_{uv}|, |A_{vu}|, |A_{vv}|\}) = 1 \quad (4)$$

and we limit our framework to cases where

$$|K| < 1 \quad (5)$$

holds. With the constraints in Eqs. (4)-(5) diffusion becomes the dominant coupling. We pose these constraints, because, within this framework, augmented transmission capabilities must not become an essential part of the SD wave propagation mechanism. Rather we assume (i) that the propagation of SD can be explained even for  $K = 0$ , but (ii) that only for  $K \neq 0$  and appropriate choices of  $A_{ij}$  and  $F$  the observed two-dimensional SD patterns are described correctly, because augmented transmission determines the specific spatial evolution of an SD wave on the two-dimensional cortical surface.

We pose one further constraint on augmented transmission, in addition to  $|A_{ij}| \leq 1$  and  $|K| < 1$ , namely on the choices of  $F$ . The operators  $F$  should be, in contrast to volume transmission, of nonlocal nature. These two constraints, summarized as *weak nonlocal coupling*, are the key to incorporating just the right amount of flexibility in this framework. The nonlocality, on one hand, addresses wiring transmission by describing the effect of the structural and functional cortical connectivity on SD, and, on the other hand, includes changes in cerebral blood flow in response to SD and how these changes are fed back to change subsequent neural activity, a feedback process termed neurovascular coupling.

Wiring transmission and neurovascular coupling can include nonlocalities in both space and time. For wiring transmission, nonlocalities in space are due to long-range lateral cortical connections, and nonlocalities in time are due to increased open probabilities of metabotropic receptors in the range of seconds after their activation. The traveling speed of action potentials along lateral cortical connections and the ionotropic synaptic transmission are, compared to the speed of SD, quasi instantaneous. Nonlocality in space for neurovascular coupling, that is, how localized the vascular response is, also referred to as the vascular point spread function, depends on which component of the vascular system is considered. While changes to capillaries, i. e., the smallest component controlled by pericytes [36], can be considered as a localized transmission in space, compared to the SD wave size, changes to arterioles and arteries have wider point spread functions. Latencies in the neurovascular coupling in the order of seconds are typical and cause nonlocalities in time. Moreover, wiring transmission and neurovascular coupling can act in combination to constitute a nonlocal transmission scheme. For example, the SD wave will activate quasi instantaneously a wide spread increase in neural activity through feed-forward and feedback cortical circuitry that induces therefore a spatially global but time-delayed neurovascular response.

In Sec. 4.5 we introduce a first special case derived from Eq. (1). This is based on the Hodgkin-Grafstein model of SD extended by inhibitor dynamics. This results in a generic model with only reaction-diffusion terms (i)-(ii). In Sec. 4.6, we consider in this generic system emerging patterns and transitions between them, in particular, transitions from spiral waves to retracting wave segments. In Sec. 5 we introduce further cases derived from Eq. (1) including a nonlocal term (iii).

#### 4.5. Extended Hodgkin-Grafstein model

The first reaction-diffusion model of SD, suggested by Hodgkin and Grafstein [27], was a single species model. It is a special case model that can be derived from our framework for  $\varepsilon = 0$ . Then it follows that rate of change  $\partial_t v = 0$  and thus the inhibitor  $v$  is simply a constant parameter. The activator agent was suggested to be extracellular potassium  $[K^+]_e$ . We continue to use  $u$  as the activator. Moreover, we want to note that this activator can also be a combination of quantities having a positive feedback loop, as shown in Fig. 4, without restricting the main idea of the Hodgkin-Grafstein model. The only assumption is

that the activator rate equation  $f(u, v)$  is a cubic function in  $u$

$$\frac{\partial u}{\partial t} = u - \frac{u^3}{3} - v + \nabla^2 u. \quad (6)$$

This model describes a bistable state in cortical ion homeostases. The smallest and the largest roots of the cubic function are stable fixed points, the lower one being identified as the physiological state, the other one as the pathological state. Furthermore, the middle root is an unstable fixed point, i. e., a threshold. The Hodgkin-Grafstein model equation (6) can be solved analytically and this provides detailed mathematical insight in the mechanism of how the pathological state invades the physiological state (see for example the textbook [37]).

We can choose suitable inhibitor dynamics from the FitzHugh-Nagumo equations [38, 39] to extend the Hodgkin-Grafstein model, i. e., to obtain a model with  $\varepsilon \neq 0$ . This way we couple Eq. (6) to another ordinary differential equation

$$\varepsilon^{-1} \frac{\partial v}{\partial t} = u + \beta - \gamma v, \quad (7)$$

where  $\beta$  and  $\gamma$  are two parameters. These parameter determine the threshold, which in the single species model (Eq. (6)) was determined by  $v$ . Usually,  $\gamma$  is set constant and then  $\beta$  is solely identified as a threshold parameter.

The FitzHugh-Nagumo equations (6)-(7) are a paradigmatic model for excitable media. An excitable medium has the capacity to propagate a sustained wave as  $u$  and  $v$  concentration profiles with a defined wave front and trailing edge through a spatially extended system. Whereas the Hodgkin-Grafstein model can just account for front propagation but not for recovery defining the dynamics in the trailing edge.

The biophysical interpretation of the variables and terms in the FitzHugh-Nagumo equations (6)-(7) is originally based on membrane dynamics in a single neuron [38, 39], because these equations were derived from the Hodgkin-Huxley model of action potentials. The interpretation of Eqs. (6)-(7) as a model for SD is thus very different. In order not to cause confusion, we call Eqs. (6)-(7) an extended Hodgkin-Grafstein model in this study, although a great body of knowledge about this generic system is published under the name FitzHugh-Nagumo model (or also under the name Bonhoeffer-van der Pol model [40, 41, 42]).

The interpretation of the terms on the right hand sides of Eqs. (6)-(7) can be directly read from Fig. 4. In Eq. (6) the first "+ $u$ " on the right hand side provides the positive self-feedback loop (dashed and dotted loops), whereas the nonlinear cubic term restricts this autocatalytic process and provides a threshold. The "- $v$ " comes from the inhibitory effect of the ion pumps (arrow with circular head between boxes marked as ion pump and ion concentration). The main other important terms (as  $\gamma$  can be set to a constant in the range  $0 \leq \gamma \leq 1$  without changing the generic behavior) are the "+ $u$ " and the  $\beta$  on the right hand side of Eq. (7). The "+ $u$ " describes positive pathway to the ion pump activity when the ion concentration is out of balance (solid arrow with pointed head starting from box marked ion gradient and terminating at box ion pump), and the parameter  $\beta$  sets, as already mentioned, the threshold.

#### 4.6. Excitability probed by dynamics of functional block

The extended Hodgkin-Grafstein model of SD as a generic reaction-diffusion model of activator-inhibitor type can explain the emergence and transition between different spatio-temporal wave patterns in two spatial dimensions, for example from re-entrant SD waves revolving around a functional block to retracting waves segments, by changing parameters in Eqs. (6)-(7). This in turn can be understood as a translation in the parameter space of this model. If we set  $\gamma$  to a constant value in the range  $0 \leq \gamma \leq 1$ , there remain only two main parameters in this set of equations, namely the time scale ratio  $\varepsilon$  of inhibitor and activator dynamics and the threshold  $\beta$ . Both parameters are closely tied to the excitable behavior, that emerges in active media. Therefore, the parameter plane  $(\varepsilon, \beta)$  can be viewed as the *excitability plane*, see Fig. 5, in which certain bifurcation lines mark the emergence of specific spatio-temporal patterns.

One axis of the excitability plane is spanned by the parameter  $\varepsilon$ . This parameter appears in Eq. (7). It is also explicitly given in the model equation (1), indicating that  $\varepsilon$  is independent on the specific model derived from the framework. It is usually a small positive number ( $0 < \varepsilon \ll 1$ ), which means that the recovery processes (arrows with circular head in Fig. 4) are slower than the autocatalytic excitation caused by positive feedback loops (dashed and dotted arrows in Fig. 4). In Fig. 5, the horizontal axis of the excitability plane is spanned by the negative logarithm of the time scale ratio  $\varepsilon$ , called time scale ratio index  $-\ln \varepsilon$ . To give an example, if  $\varepsilon = 0.1$ , the kinetic rates of the inhibitory processes are by one order of magnitude slower than those of the activator and the time scale ratio index is accordingly 1. The other parameter, that spans the vertical axis of the excitability plane in Fig. 5, is the excitation threshold, which depends on the specific model derived from the framework. In the extended Hodgkin-Grafstein model  $\beta$  can be chosen as a threshold parameter, if  $\gamma$  is set constant, for example for Fig. 5 we choose  $\gamma = 0.5$ . The units of  $\beta$  are rather arbitrary, but a characteristic value is  $\beta = 0.6$  (if  $\gamma = 0.5$ ) at which the activator-inhibitor dynamics becomes oscillatory for small  $\varepsilon$ .

In the parameter plane in Fig. 5 certain bifurcation lines mark the parameter values at which specific patterns emerge. These patterns are also seen in the experimental SD systems by monitoring the functional block (spiral tip dynamics). In fact, the dynamics of the functional block can be used to probe the tissue excitability and locate the occurrence of these patterns in the excitability plane in Fig. 5. For example, it was shown that under standard experimental condition (Sec. 2.1) the functional block of retinal SD waves is an one-dimensional curved line (inset (a) Fig. 5), which itself performs a complex rotation [22]. This is caused by a combination of effects. Essentially, a long trailing edge (indicating small  $\varepsilon$ ) causes a large refractory zone that the spiral tip, which has a high tendency to curl in (indicating small threshold  $\beta$ ), must avoid leading to complex re-entrant manoeuvres. Similar dynamics of linear functional blocks is obtained in computer simulations of the extended Hodgkin-Grafstein model (i. e., FitzHugh-Nagumo equations (6)-(7)) in a certain parameter regime close to the black full circle in Fig. 5 [43]. This regime is bounded from one side by a bifurcation line  $\partial C$  (dotted line) beyond which complex

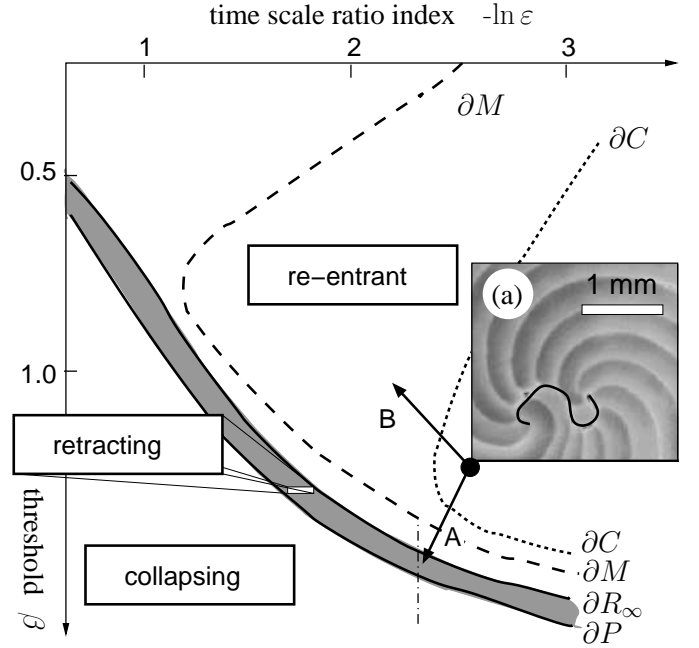


Figure 5: Parameter space of an generic active medium (FitzHugh-Nagumo equations adopted from [43]), with parameter regions separated by bifurcation lines  $\partial C$ ,  $\partial M$ ,  $\partial R_\infty$ , and  $\partial P$  that mark sudden changes in the spatio-temporal patterns from complex, meandering, rigid rotating spiral patterns, to the left of  $\partial C$ ,  $\partial M$  and  $\partial R_\infty$ , respectively, to the propagation boundary  $\partial P$ . To the left of  $\partial P$  the medium is non-excitable. The inset (a) is the predicted location of retinal spiral-shaped SD waves with a linear functional block (solid line) in the regime of complex re-entrant patterns.

rotation of largely linear functional blocks is found (to the right of  $\partial C$ ). On the other side of  $\partial C$ , simpler interactions between spiral tip and refractory zone occur and the functional block is described by a meandering pattern. This region is bounded by  $\partial M$  (dashed line). Between yet another bifurcation line,  $\partial R_\infty$  (solid), and  $\partial M$  occur reentrant patterns with a perfect circular functional block (also called rigid rotation), indicating only weak or no interactions of the re-entrant wave with its refractory trailing edge. At least, in the narrow zone  $\partial R_\infty$  and  $\partial P$  (shaded gray) only retracting wave segments occur.

## 5. Control and modulation by weak nonlocal coupling

Control and modulation of reaction-diffusion patterns by weak nonlocal coupling are the key features of the framework that provide enough flexibility to explain the experimentally observed data. In this section, we sketch principal mechanisms of nonlocal transmission that lead to the driving force and are hitherto hidden behind the nonlocal operator described by the terms  $A_{ij}F$ . This augmented transmission can explain two-dimensional wave patterns observed experimentally. The emergence of these patterns depends on this augmented transmission capabilities and would in this form not occur in a pure reaction-diffusion system of activator-inhibitor type. Many of these principles have been investigated in other active media in detail in previous studies both experimentally and theoretically. For example, two-dimensional pattern formation in the chem-



ical Belousov-Zhabotinskii reaction was studied with external feedback loops. Therefore we only outline these principles and refer to the corresponding studies for details. We begin with describing changes in excitability as translation in the excitability plane, as shown in Fig. 5, along which the excitable state can cross bifurcation lines leading to an abrupt change in the two-dimensional wave pattern (Sec. 5.1). Then, we consider the stabilization of wave segments to account for sustained propagation (Sec. 5.2), and, finally investigate re-entrant wave patterns in this framework with further reference to clinical data of persisting migraine aura without infarction (Sec. 5.3).

### 5.1. Control by long-range connections and time-delayed feedback

In this subsection, we describe the effect of long-range connections and time-delayed feedback on reaction-diffusion system of activator-inhibitor type. This was reported in detail in recent studies [44, 33]. Therefore we can limit our description to issues that are relevant to link this theoretical work to the experiments of SD waves in retina (Sec. 3.1), in particular, to the transition from spiral-shaped SD waves to SD wave segments by administering drugs (see also Sec. 4.6). In the outset of this section, we consider the efficiency of general control schemes causing translations within the excitability plane.

Let us assume, for the sake of argument, that we can deliberately control the values of the parameters  $\varepsilon$  and  $\beta$  that span the excitability plane shown in Fig. 5. Furthermore, the system is in the state marked by the black full circle in Fig. 5 and the control goal is to reach a target state being weakly susceptible to SD. In this target state, all SD waves with open ends shall retract or even collapse so that SD occurs only transiently. The whole regime of states being weakly susceptible to SD is located in the excitability plane to the left of  $\partial R_\infty$ . Between  $\partial R_\infty$  and  $\partial P$  only retracting wave segments can occur (but see also Fig. 7 because the location of the rotor boundary actually depends also on the size of the wave segment), and near but left to  $\partial P$  in Fig. 5 only collapsing waves occur. Then the seemingly simplest way to reduce tissue excitability is moving along arrow (A) in Fig. 5. The system then moves away from a location in the parameter regime of complex re-entrant patterns revolving around a linear functional block (Fig. 5, inset), i.e., from a location to the right of  $\partial C$  (dotted line), towards a state in the regime being only weakly susceptible to SD.

The efficiency of any control method that moves the system within the excitability plane, for example along arrow (A) (Fig. 5), should be defined by some optimization criterion. Path (A) is clearly better than the path along the direction of the arrow (B), because the latter path will not reach the target state, although the excitability might seem to decrease moving along the direction of path (B), if the dynamics of the functional core is used to probe excitability. The core motion becomes simpler to the left of  $\partial C$  (dotted) and again simpler crossing  $\partial M$  (dashed): from complex to meandering to rigidly rotating spiral-shaped SD waves, respectively (Sec. 4.6). This sequence of patterns can erroneously indicate that eventually the system might become weakly excitable as the same bifurcation lines need to be crossed before the target state can be reached. This generic

behavior of complex systems poses a problem, if the monitored functional core dynamics are used to probe the effect of anti-migraine drugs. The same holds if even simpler wave parameters such as the velocity are used to probe the effect of anti-migraine drugs [45, 46, 47]. Moreover, since a parameter plane has no metrical structure, other measures than comparing paths that reach the target state to those that do not are not available, in particular there is no privileged shortest path. Without further constraints there exists an infinite number of possible target states in the weakly susceptible regime.

Let us now assume that excitability can only be controlled via nonlocal transmission described by the operator  $F$ , in particular, via the influence of long-range connections or time-delayed feedback. The control parameter is then the coupling strength  $K$  in Eq. 3. We limit the nonlocal transmission types to the simplest coupling schemes with only one element of the coupling matrix  $A_{ij}$  being one and the others zero. This leads to four coupling schemes, two self-coupling schemes with  $i = j$  and two cross-coupling schemes with  $i \neq j$ . Other coupling schemes, for example diagonal coupling with  $A_{ij} = 1$  for  $i = j$  and zero otherwise, are also possible and can be treated in analogy, but the limitation to only one non-vanishing component  $A_{ij}$  provides the four simplest algebraic constraints that allows us to evaluate target states in the weakly susceptible regime of the excitability plane (Fig. 5), if the system is outside this regime.

Let the matrix element not equal to zero be denoted as  $A_{ws}$  with  $w, s \in \{u, v\}$ , so that the only augmented transmission is the following. The state from species  $s$  is used to create a nonlocal driving force  $F[s]$  that is fed back to species  $w$ .

We first consider the effect of long-range connections on a planar SD wave extending in the  $y$ -direction, so that only the propagation along the  $x$ -direction needs to be considered. Moreover, we introduce the long-range connections only in one direction pointing against the direction of wave propagation. Without loss of generality, we let the wave propagate in the negative  $x$ -direction, then this long-range connection leads to the additional term in the rate equation of specie  $w$

$$F[s(x, t)] = s(x - \delta, t) - s(x, t), \quad (8)$$

where  $\delta$  is the distance of the spatial long-range connection. This directed connectivity corresponds to anisotropic nonlocal coupling in a two dimensional active medium. The functional and structural connectivity of the cortex is realistically modeled as an anisotropic (and also inhomogeneous) medium due to the patchy nature of nonlocal horizontal cortical connections, however our motivation to introduce Eq. (8) was different. One reason is to obtain a better understanding of the results obtained in previous work [33], where isotropic nonlocal coupling have also been considered. Moreover, there is a direct analogy to local time-delayed feedback. In case of local time-delayed feedback the control force  $F$  is given by

$$F[s(x, t)] = s(x, t - \tau) - s(x, t), \quad (9)$$

where  $\tau$  is the delay time.

The common feature of the nonlocal transmission types in Eqs. (8)-(9) is that the front of the reaction-diffusion wave described by Eqs. (6)-(7) receives an additional driving force from

the cortical steady state that lies ahead of the wave (in space or time). The main idea, first introduced in Ref. [33], is to replace the nonlocal terms, that is, the time-delayed term in Eq. (9), and the space shifted term in Eq. (8), by the fixed point values  $s(x, t - \tau) = s(x + \delta, t) = s^*$  of species  $s$  for this is the state ahead of the propagating wave. For example, for the coupling scheme  $A_{vu}$  this special case derived from Eq. (1) with Eqs. (6)-(7) becomes

$$\frac{\partial u}{\partial t} = u - \frac{u^3}{3} - v + \nabla^2 u \quad (10)$$

$$\varepsilon^{-1} \frac{\partial v}{\partial t} = u + \beta - \gamma v + K(u^* - u), \quad (11)$$

which can be transformed by simple algebraic operations

$$\tilde{\varepsilon} = (1 - K)\varepsilon \quad (12)$$

$$\tilde{\beta} = (\beta + K u^*) / (1 - K) \quad (13)$$

$$\tilde{\gamma} = \gamma / (1 - K) \quad (14)$$

to the reaction-diffusion system of activator-inhibitor type Eqs. (6)-(7) with effective parameters  $\tilde{\varepsilon}$ ,  $\tilde{\beta}$ , and  $\tilde{\gamma}$ .

The effective parameters  $\tilde{\varepsilon}(K)$ ,  $\tilde{\beta}(K)$ , and  $\tilde{\gamma}(K)$  in Eqs. (12)-(14) describe a motion along a defined pathway parametrized by the coupling strength  $K$  in the parameter space of the extended Hodgkin-Grafstein model. This pathway will cross  $\partial R_\infty$  at a certain point, while another coupling scheme  $A_{ws}$  can lead to a different pathway that crosses  $\partial R_\infty$  at a different point for a different value of the coupling strength  $K$ . In fact, it can be shown that the cross coupling scheme  $A_{uv}$  leads also to Eqs. (12)-(14), only with a change in the sign of  $K$  for the latter. Therefore, the cross coupling schemes  $A_{vu}$  and  $A_{uv}$  do not differ with respect to their effect. Note, however, that whether they differ with respect to efficiency must be decided in a dimensionalized model and there the ratio  $(\varepsilon A_{vu}) / A_{uv}$  must be used to compare the relative coupling strengths of the cross coupling schemes, because the physical units must be the same (in analogy, the ratio of the diffusion coefficients  $D_v / D_u = \varepsilon \delta$ , see Sec. 4.3).

By changing the coupling strength  $K$  all three parameters are varied, therefore we cannot directly illustrate the shift in the excitability plane  $(\varepsilon, \beta)$  in Fig. 5, which is a cross-section of the full parameter space taken at  $\gamma = 0.5$ . How the effective parameters reduce susceptibility to wave propagations described by either Eqs. (12)-(14) or equations corresponding to the other coupling schemes  $A_{uu}$ ,  $A_{uv}$ , and  $A_{vv}$ , was previously investigated in detail [33].

The extended Hodgkin-Grafstein model is based on the Fitz-Hugh-Nagumo equation, so this approach describes generic responses of reaction-diffusion systems in the form of activator-inhibitor type to control by nonlocal coupling types given in Eqs. (8)-(9). We want to stress a different perspective, namely that of a control failure and the subsequent change of the cortical state that was before the failure in a state nonsusceptible to SD. An internal nonlocal cortical control mechanism in the form of  $A_{ij}F$  that renders the cortical state nonsusceptible to SD and that under pathological conditions is attenuated ( $K \rightarrow 0$ ) can drive the cortex into a state where retracting SD wave segments (weakly susceptible) occur or even re-entrant SD waves.

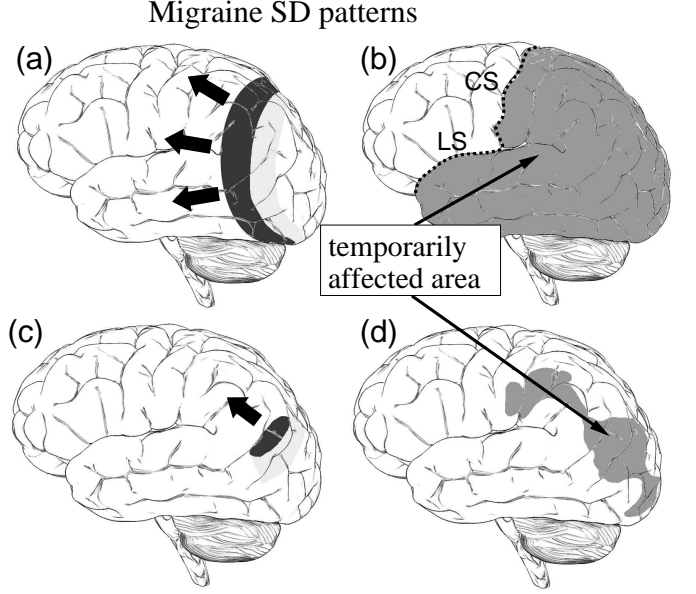


Figure 6: Paradigms of SD propagation in migraine. Current view adopted from [4]: (a) SD wave engulfing a whole hemisphere. (b) A full-scale attack affects most of the cortical surface (gray area). SD propagation is assumed to stop at the central and lateral sulcus (CS and LS, dotted line), omitting the frontal lobe (not shaded). Proposed change in paradigm: (c) localized SD wave segment affecting in a full-scale attack only a confined region of the cortex (b).

This provides a putative common mechanism of SD in migraine and stroke [44] whereas the cause of the changed control pathway can be very different for the two conditions (cf. Fig. 7 insets (a) and (b)).

## 5.2. Stabilization of wave segments

Fig. 6 (a) illustrates an SD wave that was triggered at some previous time (about 10 min earlier) in the rearmost portion of the human cortex (occipital lobe). Such figures became paradigmatic illustrations of SD wave propagation in migraine with aura, found in modern textbooks of headache [48]. This illustration made its first appearance in a seminal paper spearheading the SD theory of migraine more than 20 years ago [4]. It suggests that within a single migraine aura attack lasting about 20 min, half the cortex is transiently invaded. Fig. 6 (b) shows the spatial extent of a "full-scale attack" [4]. The wave stops in the middle, at the central and lateral sulcus (CS and LS, dotted line), and omits the frontal lobe in these illustrations. The sudden stop remains unexplained, although there are speculations in the literature suggesting "some striking metabolic difference of the two regions" [49].

The term *full-scale attack* refers to the maximal spatial extension of an SD wave in migraine. In many attacks, the SD wave will stop before. Even taking into account less severe attacks, in which SD stops earlier, it has been suggested that this paradigm illustrated in Fig. 6 (a)-(b) must be modified, namely that the maximal extent of invaded cortical tissue in a full-scale attack is far more limited (Fig. 6 (d)) caused by a localized SD wave segment (Fig. 6 (c)) [21]. The instantaneously activated area by SD in the human cortex is thus confined in its

width. From a pattern formation point of view taken within the framework of Eq. (1)-(3), this is quite a different picture revealing the presence of an additional nonlocal feedback mechanism ( $K \neq 0$ ). In the next paragraph we put forward arguments in favour of the pattern in Fig. 6 (c)-(d). The last of these arguments hints at the nature of a possibly involved nonlocal feedback represented by the operator  $F$ .

If we assume that an SD wave engulfs on its course half the cortex as shown in Fig. 6 (b), then only a subset of this activation results in sensory, e.g., visual, awareness [50]. This seems rather unlikely as the cellular depolarisation during SD is the most dramatic cortical event known. Therefore, the alternative is more likely, namely that SD in migraine occurs as a localized wave segment that within a full-scale attack affects cortical areas along certain, though variable, paths (Fig. 6 (d)). This is supported by a study investigating the sequence of neurological symptoms in migraine [51]. Moreover, similar propagation patterns were observed for the gyrencephalic feline cortex [52]: while the primary SD wave engulfed one cortical hemisphere, corresponding to Fig. 6 (b), subsequent secondary waves remained within the originating gyrus, similar to Fig. 6 (d) though more fragmented. Finally, there is one study using functional magnetic resonance imaging (fMRI) in humans during a migraine attack [5]. Although the spreading activity pattern observed by fMRI seems to support the current paradigmatic view (Fig. 6 (a)), the data is still inconclusive, as noted by Wilkinson [50], because most of the observed spreading activation could represent network activity through feed-forward and feedback circuitry but not a depolarization wave. If this is correct, the global activity in the neural circuitry, while not being part of SD, can modulate cortical susceptibility to SD. This kind of global activity is, as we will show, exactly what is needed to understand stable propagation of wave segments [53, 54, 55].

Suggesting that an SD wave in migraine takes the shape of a wave segment leads to one main problem. Wave segments are usually not solutions to reaction-diffusion systems of activator-inhibitor type, and therefore such forms, chosen as an initial condition, transform quickly. An open end of an SD wave segment either curls in to form a spiral-shape wave (Fig. 5 inset). This usually happens if cortical susceptibility to SD is rather high. To be precise, open ends of sufficiently large wave segments curl in, if the parameters  $\varepsilon$  and  $\beta$  of the system lie towards the side of the rotor boundary  $\partial R_\infty$  where the value of the threshold  $\beta$  is lower and the value of the recovery rate is slower (larger time scale ratio index  $-\ln \varepsilon$ ) than it is on the nearest point lying on  $\partial R_\infty$ . On the other side of the boundary  $\partial R_\infty$ , wave segments independent of their size retract quickly. The observed retinal SD wave patterns (Fig. 2) retract and vanished within a few millimeters (or, in temporal units, a few minutes). This is in agreement with wave segments that are based on a reaction-diffusion mechanism as described by Eqs. (6)-(7) and simulated in the weakly susceptible regime. They retract within the same order of magnitude (note that for this estimation, Eqs. (6)-(7) need to be dimensionalized, see Ref. [44].) Similar results were obtained in a descriptive mathematical model considering the motion of curves with free ends [24]. In this geometric model, spatially confined SD wave seg-

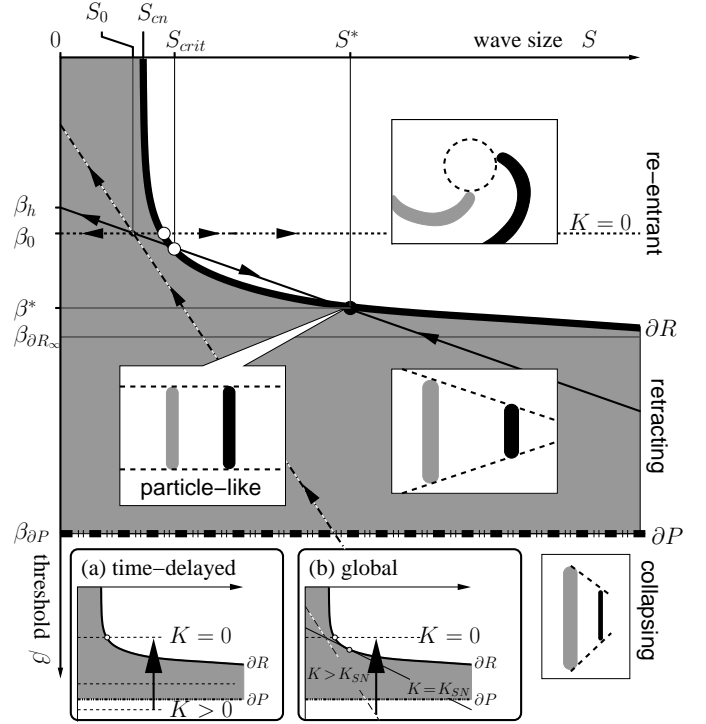


Figure 7: Scheme of the classification of excitability according to spatio-temporal patterns (re-entrant/spiral, particle-like, retracting, collapsing) in 2D along the dashed-dotted line in Fig. 5. The insets show wave front at two instances of time ( $t_1$ : gray,  $t_2$ : black) and trajectory of open wave ends (dashed). (a) The scheme illustrates a shift in the threshold by an attenuated ( $K \rightarrow 0$ ) long-range coupling or time-delayed feedback according to Eq. 13. (b) The scheme illustrates a shear of the control line from dash-dotted to solid as global feedback (Eq. 17) is attenuated ( $K \rightarrow 0$ ). At  $K = K_{SN}$  (solid line) a saddle-node bifurcation occurs.

ments were first suggested to cause aura symptoms, and it was estimated that a full-scale migraine aura attack hardly spreads more than several centimeters, and this maximal distance is only obtained if parameters are correctly adjusted.

Adhering strictly to the definition of the rotor boundary as a boundary for spiral waves, this boundary depends on the wave segment size  $S$  and is called  $\partial R$ . At any point to the right of  $\partial R_\infty$  in Fig. 5 only SD wave segments above a critical size curl in at their two open ends to form a counter-rotating double spiral wave, while those below this size retract and the wave vanishes. This can readily be deduced from the fact that the two attracting final states coexist in this parameter regime, namely the one with a counter-rotating double spiral wave and the homogeneous steady state. There is a separatrix manifold in the phase space separating the two basins of these two attractors and thereby defining a perturbation threshold. Usually, on this separatrix manifold a fixed point exists that is stable with respect to the flow parallel to this manifold. This fixed point is a saddle point in the full phase space and corresponds to an unstable solution, a so-called particle-like wave of finite size revealing a naturally shaped wave segment that only retracts or grows when perturbed. [54, 55].

The wave size  $S$  can be defined as the surface area of the wave segment where a certain elevated activator concentration

$u_e$  is exceeded

$$S(t) = \int \Theta(u(\mathbf{r}, t) - u_e) d\mathbf{r}, \quad (15)$$

where  $\Theta$  is the Heaviside function and  $\mathbf{r}$  denotes the location on the two-dimensional cortical surface. Since the wave size  $S$  is a derived system quantity, it is not represented in the parameter plane in Fig. 5, and therefore  $\partial R$  cannot be represented either. Instead, the boundary  $\partial R_\infty$  is marked as the limit of infinitely large wave segments that neither retract nor grow, so-called critical fingers [56, 57]. At  $\partial R_\infty$ , the cortical susceptibility to spiral SD waves approaches its lower bound, because arbitrarily large segments retract below this boundary and therefore waves with open ends can not re-enter and will eventually disappear.

It was shown in a chemical model system of reaction-diffusion waves experimentally and with a mathematical reaction-diffusion model [54, 55] that particle-like waves can be stabilized if the wave size  $S(t)$ , as given in Eq. (15), is used to adjust excitability  $\phi$  by the linear relation

$$\phi(t) = aS(t) + b, \quad (16)$$

where  $a$  and  $b$  are characteristic feedback parameters of this global feedback control scheme. In this chemical model system [55] the quantity  $\phi$  corresponds to the light intensity that controls the excitability of the chemical reactions, and this quantity has a similar function as  $\beta$  in the FitzHugh-Nagumo equations.

The global feedback control scheme in Eq. (16) can be translated into our framework by setting  $a = K$  and  $b = \beta_0 - KS_0$  with some reference values  $\beta_0$ ,  $S_0$  and replacing in Eq. (7) the constant parameter  $\beta$  with the controlled threshold  $\beta(t) = \phi(t) = aS(t) + b$  so that

$$\beta(t) = \beta_0 + K(S - S_0). \quad (17)$$

For  $K = 0$ , the uncontrolled FitzHugh-Nagumo inhibitor rate equation with  $\beta = \beta_0$  is obtained. The operator  $F$  is then

$$F[u(x, t)] = S(t) - S_0 \quad (18)$$

and all components of the matrix fulfill  $A_{ij} = 0$  except for  $A_{vu} = 1$ .  $S_0$  and  $K$  are, like  $a$  and  $b$  in the notation of Eq. (16), the two characteristic feedback parameters of this global feedback control scheme. In addition to these parameters, the value of  $\beta_0$  plays a central role for this global control scheme.

The meaning of  $S_0$ ,  $K$ ,  $\beta_0$ , and further related quantities can be directly read from the plane in Fig. 7. This is an illustrating scheme where the vertical axis is spanned by the controlled threshold  $\beta$  and corresponds in principle to the dash-dotted line marking a section in the parameter space at constant  $\varepsilon$  in Fig. 5. The horizontal axis is spanned by the size  $S$  of the wave segment. Note that we have dropped in the notation of  $S$  and  $\beta$  the explicit time dependence, as this is more compact. Throughout this section and in Fig. 7,  $S$  and  $\beta$  should be read as time dependent quantities. Both quantities are projections from the infinite phase space of the reaction-diffusion system, for  $S$  this projection is defined via Eq. (15) and for  $\beta$  via Eq. (17). Since  $\beta$  is a quantity derived from  $S$ , only a one-dimensional section of the  $(S, \beta)$  plane corresponds to a phase space projection of a system with parameters  $S_0$ ,  $K$ , and  $\beta_0$ , as described in the following.

Without the global coupling, i. e., for  $K = 0$ , the value of the threshold  $\beta$  does not depend on  $S$  and it is therefore constant ( $\beta = \beta_0$ ). In this case, the evolution of wave segments represented in the  $(S, \beta)$  plane is confined to a horizontal line, e. g., the thin dotted horizontal line in Fig. 7. As described in previous Sec. 5.1, the value of the threshold of the free system ( $K = 0$ ) can be in three characteristic regimes: (i) either it is in the regime where all wave profiles collapse independent of size and shape ( $\beta_0 > \beta_{\partial P}$ ), (ii) or where all wave segments retract ( $\beta_{\partial P} > \beta_0 > \beta_{\partial R_\infty}$ ), (iii) or where only wave segments below a critical size, marked by the solid thick black line  $\partial R$ , retract and if having a larger size grow to form a spiral pattern ( $\beta_0 < \beta_{\partial P_\infty}$ ). Note that a horizontal line located at  $\beta = \beta_0$  indicates the absence of a global control scheme in Fig. 7, but  $\beta_0$  can still be an effective parameter as given in Eq. (13), that is,  $\beta_0$  can be, for example, being controlled by time-delayed feedback or long-range coupling (inset (a)).

With global coupling, i. e., for  $K \neq 0$ , the threshold depends on  $S$  and the evolution of a wave segment represented in the  $(S, \beta)$  plane is then confined to an inclined line, e. g., the thin solid and dash-dotted lines with arrows. With increasing coupling strength  $K$ , the inclination with respect to the horizon increases and the line of controlled wave segment evolution is sheared along the vertical line  $S = S_0$ . So there is one invariant pivot point  $(S_0, \beta_0)$ . If this point is located at certain positions in the  $(S, \beta)$  plane, and  $\partial R$  is a convex boundary of the re-entrant wave regime, there exists a value  $K = K_{SN}$  at which the inclined line becomes tangent to  $\partial R$ . For values  $K > K_{SN}$  (dashed-dotted line, inset (b)), all wave segments retract irrespectively of their size, though the retraction will be slower than for any uncontrolled system because the threshold is lowered as the wave segment size shrinks. At  $K = K_{SN}$ , particle-like wave solutions are born in a saddle-node bifurcation.

To obtain a saddle-node bifurcation at  $K_{SN}$ , the invariant pivot point  $(S_0, \beta_0)$  must be located in either of two regimes: in the gray shaded area below the value of  $\beta_{\partial R_\infty}$ , i. e.,  $S_0 < \partial P(\beta_0)$  and  $\beta_0 < \beta_{\partial R_\infty}$  (shown in Fig. 7), where  $\partial P(\beta_0)$  denotes the projection of  $S$  onto  $\partial P$  along  $\beta_0$ ; or in the rectangular area defined by  $S_0 > S_{cn}$  and  $\beta_0 > \beta_{\partial R_\infty}$ . If the invariant pivot point  $(S_0, \beta_0)$  is located outside these regimes, again two regimes should be distinguished. If  $(S_0, \beta_0)$  is in the rectangular area defined by  $S_0 < S_{cn}$  and  $\beta_0 > \beta_{\partial R_\infty}$ , there exists neither a value of  $K$  for which the inclined line becomes tangent to  $\partial R$  nor will the inclined line of controlled wave segment evolution intersect with  $\partial R$  for  $K > 0$  and therefore particle waves cannot be stabilized. If  $(S_0, \beta_0)$  is in the white area below the value of  $\beta_{\partial R_\infty}$ , i. e.,  $S_0 > \partial P(\beta_0)$  and  $\beta_0 < \beta_{\partial R_\infty}$  there is no critical value of  $K_{SN}$  above which global control successfully blows up the basin of attraction of the homogeneous steady state to invade the whole phase space.

It is noteworthy to mention that this control adds a distinctly new character to the spatio-temporal patterns by merely changing the stability of a solution that exists in the uncontrolled system. For example, for  $K$  slightly smaller than  $K_{SN}$ , as indicated by the solid line in Fig. 7, an initial wave segment above a critical wave size  $S_{crit}$  will grow while the value of the controlled threshold  $\beta$  will simultaneously be adjusted by the global feed-

back to the final value  $\beta^*$  at which a stable particle-like wave solution of size  $S^*$  is obtained. This particle-like wave is also a solution, though unstable, of the uncontrolled system Eqs. (6)-(7) with  $\beta_0 = \beta^*$ . If, however, the initial wave segment size has a value below the critical wave size  $S_{crit}$ , the wave segment will retract and once vanished the controlled threshold  $\beta$  reaches the value  $\beta_h$  for the homogeneous state of the cortex.

There are cases where  $K$  is too large and the control becomes *too hard*. For example, for  $K = 0.1824$ ,  $\gamma = 0$ ,  $\varepsilon = 0.04$ , and  $\beta_h = \beta_0 - KS_0 = 1.721$ , we observed that particle-like waves can start to temporally *breathe*, that is, they change their size in an oscillatory fashion and reach the final target size  $S^*$  only after a long transient of several oscillations ( $> 50$ ). From this we infer that the real parts of the eigenvalues of the stable focus node, which corresponds to the stable particle-like wave solution (full black circle), become close to zero. A Hopf bifurcation that leads to stable breathing patterns, as observed in semiconductor nanostructures [58, 59, 60], which are based on similar dynamics, have, however, not been found.

It will be an important future task to relate concepts and quantities illustrated in Fig. 7 to SD in human cortex in order to develop new therapeutic methods that make use of these concepts. That Fig. 7 correctly describes the control of cortical susceptibility to SD in migraine is currently only supported by various correct predictions of such a model. Beside those mentioned in the outset of this paragraph and those reported in previous studies [24, 61, 23, 21], we note one additional prediction that shows the unifying character of this framework. So-called clinically silent migraine aura, that is, an aura that migraineurs are subjectively unaware of because they do not experience any neurological disturbance, might simply be explained by a quickly retracting SD wave patterns occurring for values  $K > K_{SN}$  (dash-dotted line). Likewise, it is known that clinically silent epilepsies are caused by seizure activity that does not break away from a focus. Our framework would still predict that the control mechanism is switched on to suppress propagation, which must result in a blood flow 'fingerprint' of SD, which indeed is observed by non-invasive imaging [14].

### 5.3. Re-entrant SD: a functional definition of tissue at risk

The re-entrant SD wave pattern observed in the experimental stroke model (Sec. 3.2) is illustrated in Fig. 8 (a): an anatomical block of nonexcitable tissue (black) develops surrounded by a ring-shaped zone becoming susceptible to SD (gray). The experimental procedure (Sec. 2.2) does not necessarily cause irrecoverable damage in the form of an infarct lesion in the core region, but there is still an anatomical block for a large central area is not affected by the cycling.

The focus in this section is on the surrounding ring-shaped zone (gray, Fig. 8 (a)). Its dynamical features are of crucial clinical interest, because the aim of stroke therapy is salvage of this tissue (Fig. 8 (b)). At the outset of this section, we consider the case that the anatomical block is an infarct core. In fact, when infarct lesions in the cerebral cortex are experimentally induced by vessel occlusion, re-entrant patterns similar to those reported here emerge [17]. By the end of this section, we will then reconsider that the anatomical block induced with

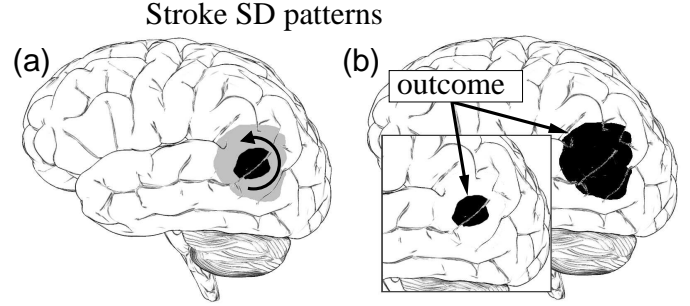


Figure 8: (a) Cortical state during a localized graded reduction in blood flow. Below a critical threshold of perfusion, an infarct lesion develops (black) surrounded by tissue becoming susceptible to SD waves (gray). These waves can spread in various patterns, e.g. radial outwards from the infarct core and cycling around it. (b) The infarct tissue may eventually include much of the surrounding tissue or be limited to the initial infarct core inset.

our experimental procedure is likely to be only nonsusceptible to SD but also salvageable, in particular, we compare the observed pattern with strikingly similar observations in persistent migraine aura without infarction.

The cortical mechanisms by which the ring-shaped zone (gray, Fig. 8 (a)) is formed are not yet fully established and consequently there is also not a clear definition of how far this zone actually spreads out. We suggest that the mathematical framework outlined in Eq. 1 can complement current clinical definitions of this spatial structure. The zone surrounding an infarct core is either called penumbra [62], denoting a concept based on a decreased blood flow range, or an alternative concept is based on the tissue at risk of infarction being potentially salvageable. In stroke outcome, the infarct tissue may eventually include much of the surrounding tissue (Fig. 8 (b)) or be limited to the initial infarct core (Fig. 8 (b) inset).

The *tissue-at-risk* (TAR) concept is clinically most relevant, but it does not formulate a distinctive definition. This concept must be substantiated by what processes underlie this risk so that it becomes clear what constitutes high and low-risk. A decreased blood flow range is one possible substantiation, which, if the sole complement, would identify the penumbra as TAR. The penumbra is anatomically defined. By contrast TAR can also be defined as a functional concept in terms of nonlinear dynamics [23]. In its original functional form, TAR was suggested to extend over the area invaded by transient waves occurring below the propagation boundary (to the right of  $\partial P$  (Fig. 5)). This functional definition did not incorporate a gradient in susceptibility caused by anatomical heterogeneities. We suggest in the following to combine these anatomical and functional concepts, which would then attach great clinical importance to re-entrant pattern.

The defining property of re-entrant pattern with an anatomical block is the heterogeneity. In stroke, this heterogeneity is evolving and occurs actually over several scales. On the largest scale is the infarct core and the surrounding region. In the infarct core blood supply is below the threshold of energy failure, outside it is constrained but the energy state is preserved. On a smaller scale occurs a heterogeneous microcirculation [63, 62].

A mathematical model that does not incorporate a complete characterization of this heterogeneous microcirculation can use nonlocal terms to describe the macroscopic spatial connectivity in form of a network of local excitable elements described by Eqs. (6-7)). In such a model [64, 65], it was shown that spatial diversity induces wave patterns. Diversity is able to induce a transition to an excitable behavior of the net. These patterns are most coherent for an intermediate variability strength, an effect that is described as similar to stochastic resonance generated by additive noise.

The spatio-temporal pattern reported in Sec. 3.2 are strikingly reminiscent of patterns reported by migraineurs suffering from a rare but well documented subform of migraine classified as *persistent migraine aura without infarction* in the second edition of the international headache classification (ICHD-II code 1.5.3). In this subform, migraine aura phenomena, which are otherwise transient neurological symptoms lasting less than 30 min, persist for more than 1 week, maybe months or years. To diagnose this subform, there must not be any evidence by noninvasive imaging of an infarct and these symptoms must not be attributed to another disorder. In Fig. 9 (a) a persistent central visual disturbance is illustrated. The scotoma is filled by geometric pseudohallucinations of lattice form. While this pattern is seen always, even with eyes closed during an acute migraine attack the size of central scotoma can decrease and become up to 4 times larger (Fig. 9 (b)), or a further disturbance can propagate in one visual hemifield (c) or in both (d).

In analogy to the stabilization of particle-like waves described in Sec. 5.2, these stationary patterns might be explained by the stabilization of a critical nucleus with global feedback. The critical nucleus refers to a spatially confined structure lying in the phase space on the separatrix manifold separating the basins of attraction of a ring-shaped wave and the homogeneous steady state. It defines a stationary radial symmetric perturbation threshold, while the particle-like wave is a traveling asymmetric perturbation threshold. The stabilization of the critical nucleus can probably not be achieved by global feedback as introduced in Eq. (18), because the coupling strength must be very large. A large inclination of the control line in Fig. 7 can be predicted if assuming that the particle-like wave size approaches the size of the critical nucleus  $S_{cn}$  for small thresholds. However, if the operator  $F$  has a nonlinear dependence on  $S$ , or additional long-range, time-delayed, and other nonlocal augmented transmission schemes, including spatial diversity, are considered in combination with reaction-diffusion, a rich repertoire opens up and it will be an important task for future research to investigate this in the context of migraine and stroke patterns.

## 6. Discussion and outlook

We have presented a mathematical framework for cortical spreading depolarizations that unifies existing activator-inhibitor models as special cases [27, 28, 29, 30, 31]. Within this framework the reaction-diffusion mechanism of SD is extended by nonlocal coupling as an integral part of the phenomenon necessary to describe the emergence and transitions of two-dimensional

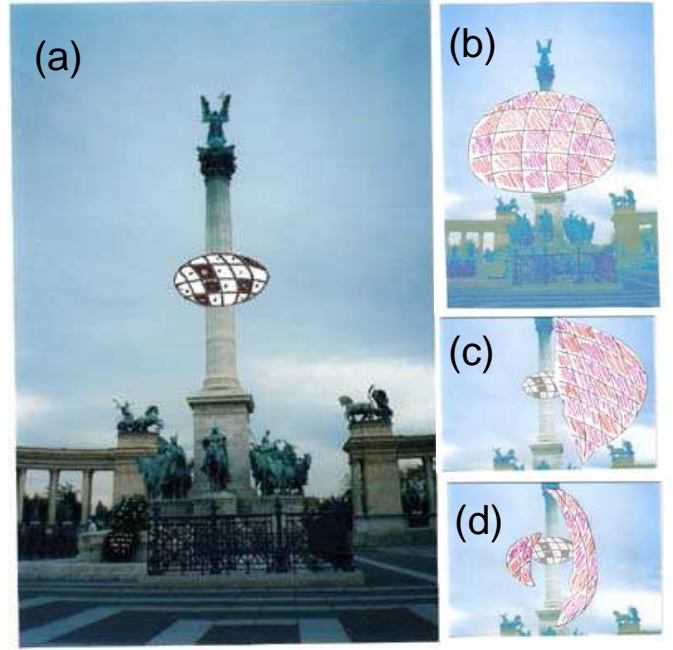


Figure 9: (a) Persistent central scotoma seen with open eyes. The area of the central scotoma is filled by geometric hallucinations of lattice form dimension. The pattern in this area remains when eyes are closed. During a migraine attack starting from the central scotoma various patterns can occur. (b) Expanding the initial affected area in the visual field, (c) waves propagation in one visual hemifield, and (d) waves propagating in both visual hemifields.

SD wave patterns. As a framework it provides a flexible procedure for analysing SD patterns observed in both experimental migraine and stroke models, and clinical data [5, 11].

This framework is aimed at providing basic insights needed to understand cortical susceptibility to transient SD wave propagation in terms of nonlinear science. In particular, we focus on bifurcations in the dynamics of cortical homeostasis caused by cortical circuits and neurovascular coupling represented as nonlocal transmission schemes. A long term goal is to provide control strategies based on bifurcation theory for both traditional pharmacological treatments and biomedical engineered devices that intelligently target the occurrence of SD waves.

A mathematical model that involves only two species with activator-inhibitor dynamics is undoubtedly a very crude macroscopic level of cortical homeostasis. Activator-inhibitor dynamics is the minimal requirement that leads to a description of SD as a traveling wave pattern with a trailing edge. In two spatial dimensions, these waves take a characteristic form that reveals much about cortical susceptibility to SD. Yet, little insight into microscopic mechanisms of SD is offered by such minimal dynamic systems. There are much more sophisticated mathematical descriptions of SD on a detailed microscopic level that try to resolve the mechanism of SD [66, 67]. In our framework, these microscopic mechanism are hidden inside the box labeled as "firing rate" (Fig. 4).

Proposing a conceptual framework at this macroscopic level must be justified by showing that this approach avoids deficiencies that would arise if SD wave propagation is modeled on a

microscopic level. From the clinical perspective, the macroscopic scale, in particular, the two-dimensional pattern on the cortical surface, is highly relevant. In migraine, the whole spectrum of aura subtypes could depend critically on whether SD can break away from a focus point, and, if it does, whether SD waves take the shape of a particle-like wave and therefore limit the extent of a full-scale attack to certain cortical regions (Fig. 6 (d)), or, in the worst case, SD becomes a persistent activity pattern (Fig. 9). In stroke, outcome depends on SD as these waves are suspected to contribute to the loss of potentially salvageable tissue, i. e., tissue at risk of infarction. Since re-entrant pattern increase the total number of waves, the emergence of these patterns need to be understood. None of these questions can be addressed in a cellular model of SD including only one or several neurons, let alone the semantic objection against applying the term *spreading* to such models because they are not meant to model the spread [12].

Microscopic models include several ion channel types in a single neuron, and its dendritic tree. These models also consider surrounding compartments, and can therefore also describe changes in intra- and extracellular ion concentrations [66, 67]. To obtain the continuum limit of such discrete microscopic cellular models is by no means straightforward. The problem is to match the very detailed and accurate knowledge of microscopic processes involved in the depolarization cycle of SD by an equally detailed description of volume transmission and wiring transmission needed to provide the spatial coupling for transition to the continuum limit. Mismatching these levels of description by merely using a diffusion term as in Eq. (2) to simulate spatial coupling by extracellular potassium would be like attaching the wheels of a carriage on a Mercedes.

Efforts have been made to address this problem by accounting not only for interstitial ionic diffusion but also for ionic movement through a neuronal syncytium of cells connected by gap junctions and for cells that are allowed to expand in response to osmotic pressure. From these it was concluded that cytosolic diffusion via gap junctions and osmotic forces are important mechanisms underlying SD [68]. Yet, to compute the spatio-temporal development of SD across the cortical surface on a centimeter scale and investigate the emergence of retracting, re-entrant, and stationary SD waves, coupling schemes other than local schemes must be accounted for. There are important nonlocal transmission schemes in the cortex that provide spatial coupling over a long range or lead to time delays. Example are (i) the functional and structural cortical connectivity, in the continuum limit described by neural fields [69], (ii) the cortical energy state maintained by a segmental blood perfusion from the arteries to smaller arterioles and finally branching capillaries leading to a complex hemodynamic response that is regulated by smooth muscle cells (arterioles) and pericytes (capillaries) [36], and (iii) the topology of the network of the neuronal syncytium that will be compromised by disseminate neuronal injury during ischemia [70]. There are more transmission schemes, but the effect of these (i)-(iii) are the ones we have considered in a first approximation by (i) long-range connections, (ii) global coupling, and (iii) spatial diversity.

Future investigations have to relate the quantitative values

of the parameters in macroscopic model that successfully describe the bifurcations observed in the spatio-temporal characteristics of SD to the cellular level. This will open up this approach for the design of both drug treatments [23] and engineered devices utilizing transcranial stimulation [71] with the aim to target SD intelligently. Migraine and stroke are found in specific genetic disorders giving clues to genetic factors that hint at differences in the cortical network activity. Such hints may provide means to bridge the gap between the macroscopic and microscopic level of SD. Similar hints of changed network activity are coming from psychophysics describing abnormal cortical processing in migraine by concepts like hyper- and hypoexcitability, heightened responsiveness, a lack of habituation and/or a lack of intra-cortical inhibition [72, 50]. Our framework provides means by which such statements on cortical excitability in migraine can be investigated, in particular how abnormal cortical nonlocal connectivity changes susceptibility to SD. Although it seems tempting to suggest that cortical hyperexcitability increases susceptibility to SD or even that neurons prone to hyperexcitability trigger SD, such a simple relation cannot be expected, and a detailed bifurcation analysis will be important for the thorough understanding of SD as a nonlinear pattern formation process.

## References

- [1] D. W. Dodick and J. J. Gargus: *Why migraines strike*, Sci. Am. **299**, 56 (2008).
- [2] A. A. P. Leão: *Spreading depression of activity in the cerebral cortex*, J. Neurophysiol. **7**, 359 (1944).
- [3] P. M. Milner: *Note on a possible correspondence between the scotomas of migraine and spreading depression of Leão*, Electroencephalogr. Clin. Neurophysiol. **10**, 705 (1958).
- [4] M. Lauritzen: *Cortical spreading depression as a putative migraine mechanism*, Trends in Neurosciences **10**, 8 (1987).
- [5] N. Hadjikhani, M. Sanchez Del Rio, O. Wu, D. Schwartz, D. Bakker, B. Fischl, K. K. Kwong, F. M. Cutrer, B. R. Rosen, R. B. Tootell, A. G. Sorensen, and M. A. Moskowitz: *Mechanisms of migraine aura revealed by functional MRI in human visual cortex*, Proc. Natl. Acad. Sci. USA **98**, 4687 (2001).
- [6] M. A. Moskowitz: *The 2006 Thomas Willis lecture: the adventures of a translational researcher in stroke and migraine*, Stroke **38**, 1645 (2007).
- [7] K. A. Hossmann: *Periinfarct depolarizations*, Cerebrovasc. Brain Metab. Rev. **8**, 195 (1996).
- [8] A. J. Strong, M. Fabricius, M. G. Boutelle, S. J. Hibbins, S. E. Hopwood, R. Jones, M. C. Parkin, and M. Lauritzen: *Spreading and synchronous depressions of cortical activity in acutely injured human brain*, Stroke **33**, 2738 (2002).
- [9] M. Fabricius, S. Fuhr, R. Bhatia, M. Boutelle, P. Hashemi, A. J. Strong, and M. Lauritzen: *Cortical spreading depression and peri-infarct depolarization in acutely injured human cerebral cortex*, Brain **129**, 778 (2006).
- [10] J. P. Dreier, J. Woitzik, M. Fabricius, R. Bhatia, S. Major, C. Drenckhahn, T.-N. Lehmann, A. Sarrafzadeh, L. Willumsen, J. A. Hartings, O. W. Sakowitz, J. H. Seemann, A. Thieme, M. Lauritzen, and A. J. Strong: *Delayed ischaemic neurological deficits after subarachnoid haemorrhage are associated with clusters of spreading depolarizations*, Brain **129**, 3224 (2006).
- [11] C. Dohmen, O. W. Sakowitz, M. Fabricius, B. Bosche, T. Reithmeier, R. I. Ernestus, G. Brinker, J. P. Dreier, J. Woitzik, A. J. Strong, and R. Graf: *Spreading depolarizations occur in human ischemic stroke with high incidence*, Ann. Neurol. **63**, 720 (2008).
- [12] G. G. Somjen: *Mechanisms of spreading depression and hypoxic spreading depression-like depolarization*, Physiol. Rev. **81**, 1065 (2001).

- [13] J. Olesen, L. Friberg, T. S. Olsen, A. R. Andersen, N. A. Lassen, P. E. Hansen, and A. Karle: *Ischaemia-induced (symptomatic) migraine attacks may be more frequent than migraine-induced ischaemic insults*, *Brain* **116**, 187 (1993).
- [14] M. A. Moskowitz: *Defining a pathway to discovery from bench to bedside: the trigeminovascular system and sensitization*, *Headache* **48**, 688 (2008).
- [15] N. L. Peixoto, V. M. Fernandes de Lima, and W. Hanke: *Correlation of the electrical and intrinsic optical signals in the chicken spreading depression phenomenon*, *Neurosci. Lett.* **299**, 89 (2001).
- [16] A. K. Dunn, H. Bolay, M. A. Moskowitz, and D. A. Boas: *Dynamic imaging of cerebral blood flow using laser speckle*, *J. Cereb. Blood Flow Metab.* **21**, 195 (2001).
- [17] A. J. Strong, P. J. Anderson, H. R. Watts, D. J. Virley, A. Lloyd, E. A. Irving, T. Nagafuji, M. Ninomiya, H. Nakamura, A. K. Dunn, and R. Graf: *Peri-infarct depolarizations lead to loss of perfusion in ischaemic gyrencephalic cerebral cortex*, *Brain* **130**, 995 (2007).
- [18] V. M. F. de Lima, M. Goldermann, and W. Hanke: *The retinal spreading depression* (Shaker Verlag, Aachen, 1999).
- [19] M. A. Dahlem and S. C. Müller: *Image processing techniques applied to excitation waves in the chicken retina*, *Methods* **21**, 317 (2000).
- [20] R. F. Miller: *Cell communication mechanisms in the vertebrate retina the proctor lecture*, *Invest. Ophthalmol. Vis. Sci.* **49**, 5184 (2008).
- [21] M. A. Dahlem and N. Hadjikhani: *Migraine aura: retracting particle-like waves in weakly susceptible cortex*, *PLoS ONE* (2008), accepted.
- [22] M. A. Dahlem and S. C. Müller: *Self-induced splitting of spiral-shaped spreading depression waves in chicken retina*, *Exp. Brain Res.* **115**, 319 (1997).
- [23] M. A. Dahlem, F. M. Schneider, and E. Schöll: *Efficient control of transient wave forms to prevent spreading depolarizations*, *J. Theo. Biol.* **251**, 202 (2008).
- [24] M. A. Dahlem and S. C. Müller: *Migraine aura dynamics after reverse retinotopic mapping of weak excitation waves in the primary visual cortex*, *Biol. Cybern.* **88**, 419 (2003).
- [25] M. Shibata and J. Bures: *Reverberation of cortical spreading depression along closed-loop pathways in rat cerebral cortex*, *J. Neurophysiol.* **35**, 381 (1972).
- [26] J. McCulloch, L. Edvinsson, and P. Watt: *Comparison of the effects of potassium and pH on the calibre of cerebral veins and arteries*, *Pflugers Arch.* **393**, 95 (1982).
- [27] B. Grafstein: *Neural release of potassium during spreading depression*, in *Brain Function. Cortical Excitability and Steady Potentials*, edited by M. A. B. Brazier (University of California Press, Berkeley, 1963), pp. 87–124.
- [28] H. C. Tuckwell: *Simplified reaction-diffusion equations for potassium and calcium ion concentrations during spreading cortical depression*, *Int. J. Neurosci.* **12**, 95 (1981).
- [29] J. A. Reggia and D. Montgomery: *Modeling cortical spreading depression*, *Proc. Annu. Symp. Comput. Appl. Med. Care* pp. 873–877 (1994).
- [30] J. A. Reggia and D. Montgomery: *A computational model of visual hallucinations in migraine*, *Comput. Biol. Med.* **26**, 133 (1996).
- [31] M. A. Dahlem and S. C. Müller: *Reaction-diffusion waves in neuronal tissue and the window of cortical excitability*, *Ann. Phys.* **13**, 442 (2004).
- [32] E. M. Izhikevich: *Neural excitability, spiking and bursting*, *Int. J. Bifurcation Chaos* **10**, 1171 (2000).
- [33] F. M. Schneider, E. Schöll, and M. A. Dahlem: *Controlling the onset of traveling pulses in excitable media by nonlocal spatial coupling and time delayed feedback*, *Chaos* (arXiv:0812.3497) (2009), accepted.
- [34] L. F. Agnati, M. Zoli, I. Strömberg, and K. Fuxe: *Intercellular communication in the brain: wiring versus volume transmission*, *Neuroscience* **69**, 711 (1995).
- [35] E. Syková and C. Nicholson: *Diffusion in brain extracellular space*, *Physiol. Rev.* **88**, 1277 (2008).
- [36] C. M. Peppiatt, C. Howarth, P. Mobbs, and D. Attwell: *Bidirectional control of CNS capillary diameter by pericytes*, *Nature* **443**, 700 (2006).
- [37] H. R. Wilson: *Spikes, Decisions, and Actions: The Dynamical Foundations of Neuroscience* (Oxford University Press, Oxford, 1999).
- [38] R. FitzHugh: *Impulses and physiological states in theoretical models of nerve membrane*, *Biophys. J.* **1**, 445 (1961).
- [39] J. Nagumo, S. Arimoto, and S. Yoshizawa: *An active pulse transmission line simulating nerve axon*, *Proc. IRE* **50**, 2061 (1962).
- [40] B. van der Pol: *On relaxation oscillations*, *Phil. Mag.* **2**, 978 (1926).
- [41] B. van der Pol and J. van der Mark: *The heart beat considered as a relaxation oscillation and an electrical model of the heart*, *Arch. Neerl. Physiol.* **14**, 418 (1929).
- [42] K. F. Bonhoeffer: *Activation of passive iron as a model for the excitation of nerve*, *J. Gen. Physiol.* **32**, 69 (1948).
- [43] A. T. Winfree: *Varieties of spiral wave behaviour: An experimentalist's approach to the theory of excitable media*, *Chaos* **1**, 303 (1991).
- [44] M. A. Dahlem, F. M. Schneider, and E. Schöll: *Failure of feedback as a putative common mechanism of spreading depolarizations in migraine and stroke*, *Chaos* **18**, 026110 (2008).
- [45] M. Wiedemann, V. M. de Lima, and W. Hanke: *Effects of antimigraine drugs on retinal spreading depression*, *Naunyn Schmiedebergs Arch. Pharmacol.* **353**, 552 (1996).
- [46] S. Brand, V. M. Fernandes de Lima, and W. Hanke: *Pharmacological modulation of the refractory period of retinal spreading depression*, *Naunyn Schmiedebergs Arch. Pharmacol.* **357**, 419 (1998).
- [47] D. Scheller, F. Tegmeier, and W. R. Schlue: *Dose-dependent effects of tetraethylammonium on circling spreading depressions in chicken retina*, *J. Neurosci. Res.* **51**, 85 (1998).
- [48] S. D. Silberstein, A. Stiles, and W. B. Young (Editors): *Atlas of Migraine and Other Headaches* (Taylor & Francis, London, 2005).
- [49] C. S. Rebert: *Spreading depression in squirrel monkey lissencephalic cortex*, *Physiology & Behavior* **5**, 239 (1967).
- [50] F. Wilkinson: *Auras and other hallucinations: windows on the visual brain*, *Prog. Brain Res.* **144**, 305 (2004).
- [51] M. Vincent and N. Hadjikhani: *Migraine aura and related phenomena: beyond scotomata and scintillations*, *Cephalalgia* **27**, 1368 (2007).
- [52] M. F. James, M. I. Smith, K. H. Bockhorst, L. D. Hall, G. C. Houston, N. G. Papadakis, J. M. Smith, A. J. Williams, D. Xing, A. A. Parsons, C. L. Huang, and T. A. Carpenter: *Cortical spreading depression in the gyrencephalic feline brain studied by magnetic resonance imaging*, *J. Physiol. (Lond.)* **519 Pt 2**, 415 (1999).
- [53] K. Krischer and A. Mikhailov: *Bifurcation to traveling spots in reaction-diffusion systems*, *Phys. Rev. Lett.* **73**, 3165 (1994).
- [54] T. Sakurai, E. Mihaliuk, F. Chirila, and K. Showalter: *Design and control of wave propagation patterns in excitable media*, *Science* **296**, 2009 (2002).
- [55] E. Mihaliuk, T. Sakurai, F. Chirila, and K. Showalter: *Feedback stabilization of unstable propagating waves*, *Phys. Rev. E* **65**, 065602 (2002).
- [56] A. Karma: *Universal limit of spiral wave propagation in excitable media*, *Phys. Rev. Lett.* **66**, 2274 (1991).
- [57] V. Hakim and A. Karma: *Theory of spiral wave dynamics in weakly excitable media: asymptotic reduction to a kinematic model and applications*, *Phys. Rev. E* **60**, 5073 (1999).
- [58] E. Schöll: *Nonlinear spatio-temporal dynamics and chaos in semiconductors* (Cambridge University Press, Cambridge, 2001).
- [59] G. Stegemann and E. Schöll: *Two-dimensional spatiotemporal pattern formation in the double-barrier resonant tunneling diode*, *New J. Phys.* **9**, 55 (2007).
- [60] E. Schöll: *Pattern formation and time-delayed feedback control at the nano-scale*, in *Nonlinear Dynamics of Nanosystems*, edited by G. Radons, B. Rumpf, and H. G. Schuster (Wiley-VCH, Weinheim, 2009).
- [61] M. A. Dahlem and E. P. Chronicle: *A computational perspective on migraine aura*, *Prog. Neurobiol.* **74**, 351 (2004).
- [62] K.-A. Hossmann: *Pathophysiology and therapy of experimental stroke*, *Cell. Mol. Neurobiol.* **26**, 1055 (2006).
- [63] E. Leniger-Follert and D. W. Lübbers: *Regulation of microflow and behaviour of local tissue Po<sub>2</sub> during activation and anoxia of the brain cortex*, *Bibl Anat* pp. 345–349 (1977).
- [64] E. Glatt, M. Gassel, and F. Kaiser: *Variability-induced transition in a net of neural elements: From oscillatory to excitable behavior*, *Phys. Rev. E* **73**, 066230 (2006).
- [65] E. Glatt, M. Gassel, and F. Kaiser: *Variability-sustained pattern formation in subexcitable media*, *Phys. Rev. E* **75**, 026206 (2007).
- [66] H. Kager, W. J. Wadman, and G. G. Somjen: *Simulated seizures and spreading depression in a neuron model incorporating interstitial space and ion concentrations*, *J. Neurophysiol.* **84**, 495 (2000).
- [67] J. Makarova, J. M. Ibarz, S. Canals, and O. Herreras: *A steady-state model of spreading depression predicts the importance of an unknown conductance in specific dendritic domains*, *Biophys. J.* **92**, 4216 (2007).



- [68] B. E. Shapiro: *Osmotic forces and gap junctions in spreading depression: a computational model*, J. Comput. Neurosci. **10**, 99 (2001).
- [69] H. R. Wilson and J. D. Cowan: *A mathematical theory of the functional dynamics of cortical and thalamic nervous tissue.*, Kybernetik **13**, 55 (1973).
- [70] S. Hanyu, U. Ito, Y. Hakamata, and I. Nakano: *Topographical analysis of cortical neuronal loss associated with disseminated selective neuronal necrosis and infarction after repeated ischemia*, Brain Res. **767**, 154 (1997).
- [71] D. Liebetanz, F. Fregni, K. K. Monte-Silva, M. B. Oliveira, A. Amânci-dos Santos, M. A. Nitsche, and R. C. Guedes: *After-effects of transcranial direct current stimulation (tDCS) on cortical spreading depression*, Neurosci. Lett. **398**, 85 (2006).
- [72] A. J. Shepherd: *Increased visual after-effects following pattern adaptation in migraine: a lack of intracortical excitation?*, Brain **124**, 2310 (2001).

## Acknowledgement

We would like to thank Steve Coombes, Felix Schneider, Oscar Herreras, Hannelore Rittmann-Frank, Henry Tuckwell, Anthony Gardner-Medwin, and Wyste Wadman for fruitful discussions at the Nottingham migraine meeting, and Vladimir Zykov for comments on particle-like waves. MAD was supported by the Deutsche Forschungsgemeinschaft (DA 602/1-1 and SFB 555)